EPIC-pn Energy Scale for Small Window Mode: long-term CTI correction

XMM-SOC-CAL-SRN-0366

Ivan Valtchanov, Michael Smith, Norbert Schartel (ESAC)

March 29, 2019

1 CCF components

Name of CCF	VALDATE	EVALDATE	Blocks changed	CAL version	XSCS flag
EPN_CTI_0049.CCF	2000-01-01T00:00:00		LONG_TERM_CTI	3.240	NO
EPN_CTI_0050.CCF	2000-03-23T05:00:00		LONG_TERM_CTI	3.240	NO

2 Changes

The long-term charge-transfer inefficiency (LTCTI) correction is updated with the analysis of EPIC-pn observations in Small Window mode (PN-SW). Previously, the correction was based on Full Frame mode observations of the calibration source (*CalClosed* or CC mode), see [8] for details.

In the current analysis we use both observations in CC mode and of sky sources (AGNs) with narrow neutral fluorescent Fe K_α (6.4 keV rest-frame) line. Based on the results we have updated the PN-SW correction at 5.8988 keV and added a new empirical curve at energy 6.4 keV.

The updated LTCTI correction described in this report is only for PN-SW mode.

3 Energy Scale for EPIC-pn in Small Window mode

3.1 Sample

We use a subset of 16 out of all 51 *CalClosed* observations of PN in Small Window Mode, discarding a large number of observations before revolution 200, as many of them show deviant results in both CTI and no-CTI corrected spectra. The last CC observation is from XMM-Newton revolution 3242.

To include an additional energy scale point, we have added sky sources (AGN) with narrow Fe Kα (6.4 keV) line observed in PN-SW. The list of the targets and observations included in the analysis is provided in Table 1. We discard observations when the AGN is in a state where the line is either too faint or too complex. The final number of AGN observations included in the study is 21. The most recently observed one is NGC 3783, 0780860901, during revolution 3115.

3.2 Processing steps

We process all observations with XMM-SASv17 and the current calibration files.

For CalClosed observations we have the following steps:

1. `epchain withctilongterm=Y|N withphagaincolumn=yes propagatecolumns=yes`
2. Extract a spectrum from a box, avoiding the edges, and filter flags and patterns as follows:
   ```
   (DETX,DETY) in BOX(517,1430,2500,2250,0) &&
                FLAG == 0 && PATTERN == 0 && PAT_SEQ == 0
   ```
   and we use spectral channels from 0 to 20479.
3. With `specgroup` but no grouping we attach an RMF from the PN-SW canned response matrices and also an ARF from a non CalClosed PN-SW observation. And we set the `BACKFILE` FITS header keyword to NONE. This is necessary for the next step.

4. Using `XSPEC`, we fit a four-component model (power-law and 3 Gaussian lines), for the three strong lines in CalClosed observations: Al K_α (1.486 keV), Mn K_α[1] (5.8988 keV) and Mn K_β (6.490 keV) from the on-board radioactive Iron-55 calibration source. As the source decays, the Mn K_β line is becoming too faint in recent observations and we have not used it in the analysis, although we use it to check the results. The XSPEC fit uses the raw unbinned spectrum. A couple of examples of the fitting are shown in Appendix A.

The workflow for the AGNs is as follows:

1. `epchain withctilongterm=Y|N`
2. Filtering the event lists with `(#XMMEA_EP && GTI && PI > 150)`.
3. Creating an image in band [2,10] keV and manually define the source and background regions, both circles with radius 640 (32 arcsec).
4. Extract source spectrum and background, using an additional filter with `(FLAG == 0 && PATTERN <= 4)`, and use spectral channels from 0 to 20479 and set `spectralbinsize=5`.
5. Generate an RMF and ARF files.
6. Create two versions of each spectrum: one raw and one grouped with a minimum 25 counts per spectral bin. We always use the un-grouped spectra for the XSPEC fit (next step), while the grouped one is available only for consistency checks.
7. Using `XSPEC`, we fit a simple two-component model (Gaussian line + power-law continuum) limiting the spectral energy range in [4-8] keV. We always keep the line width fixed at 10 eV and set an initial estimate of the line centre at 6.3 keV. For some AGN observations the simple model was not a good description of the data (complex Fe Kα) and we simply discarded those. The XSPEC fit results for the AGNs are listed in Table 2 in Appendix B, where we also show figures with the input data, the best fit model and the ratio.

3.3 Results using the current long-term CTI correction

The difference between the best-fit line centre and the expected energy for Mn Kα (CC) and Fe Kα (AGN) lines, using spectra produced with the current calibration files (v48), is shown in Figure 1. Clearly for PN-SW, Mn K_α line centroid starts to deviate significantly (> 20 eV) from the expected energy starting at revolutions ~ 1500 ($t > 8$ years or early 2008) and reaching ~ 50 eV for the most recent observations. The offset is systematic and always towards higher energy of the line. The same behaviour, although with much larger spread, is observed using the Fe K_α line (at 6.4 keV) for a set of sources with AGN.

The results seem correct for Al Kα, so we are not going to consider it any further in the analysis and we shall keep the LTCTI tabulated function as it is now.

The results clearly show that the current long-term CTI correction, derived from Full Frame mode observations is not appropriate for Small Window mode for energies above 5.9 keV. Therefore we proceed with the steps necessary to update the calibration file with a proper correction for this mode.

3.4 Deriving the new LTCTI correction

Since the implementation of EPN_CTI_0047.CCF (and EPN_CTI_0048.CCF) in XMM-SAS v15, the LTCTI correction is provided as a tabulated function at each year since 01-01-2000T00:00:00 (t_0). The XMM-SAS then linearly interpolates to obtain the correction at the time of the observation relative to t_0. This strategy allows for a more flexible approach, as in general the time and energy dependence of the correction may not be described sufficiently well with analytical functions (e.g. a polynomial).

[1] What we call Mn K_α is actually a doublet with Mn $K_{\alpha1}$ at 5.888 keV with probability 0.162 and Mn $K_{\alpha2}$ at 5.899 keV with probability 0.6; the line centroid we use in this analysis, at 5.8988 keV, corresponds to the main component and the value used in the previous CTI analysis.

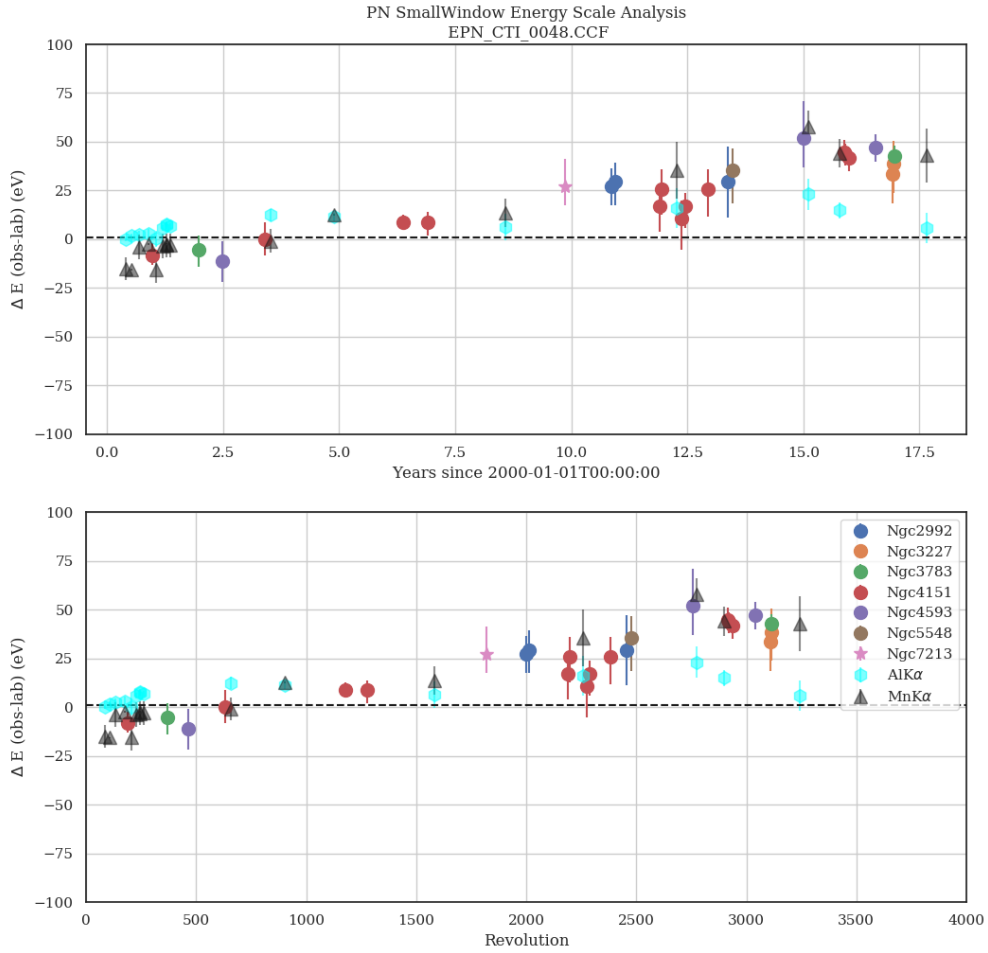

Figure 1: The difference between the expected line energy and the best fit line centre as a function of time since 2000-01-01 (top) and the XMM-Newton revolution (bottom) for PN observations in Small Window mode. All observations, AGN and CalClosed, were processed with the current calibration files: EPN_CTI_0047.CCF and EPN_CTI_0048.CCF.

To derive the LTCTI for PN-SW we reprocess all CalClosed and AGN observations, switching off the long-term CTI correction during the `epchain` steps (step 1 for both CC and AGN, with `withctilongterm=N`). And we perform exactly the same steps as explained above and extract non-CTI corrected spectra and fit the lines. Once we have all the line centroid measurements (and their uncertainties) we proceed as follows.

The correction we want to derive, LTCTI, is a function of time (t), the distance from the read-out node (RAWY) and the photon energy (E_{obs}). We can write:

$$E_{obs} = E'_{lab} \times \mathrm{LTCTI}(t, E_{ref}, \mathrm{RAWY}), \tag{1}$$

where t is the time in years relative to t_0, E_{obs} is the measured line centroid, $E'_{lab} = E_{lab}/(1+z)$ is the redshifted line energy of the line rest-frame E_{lab}, z is the redshift and E_{ref} is the reference energy for which we have derived the LTCTI. For CC observations $z = 0$, while for the AGNs it is listed in Table 1.

In the current calibration file for PN-SW we have two reference curves for E_{ref} at 1.486 keV (Al Kα) and E_{ref} at 5.8988 keV (Mn Kα). XMM-SAS then linearly interpolates the two curves to derive the correction for the each individual event energy and time. The interpolation in energy

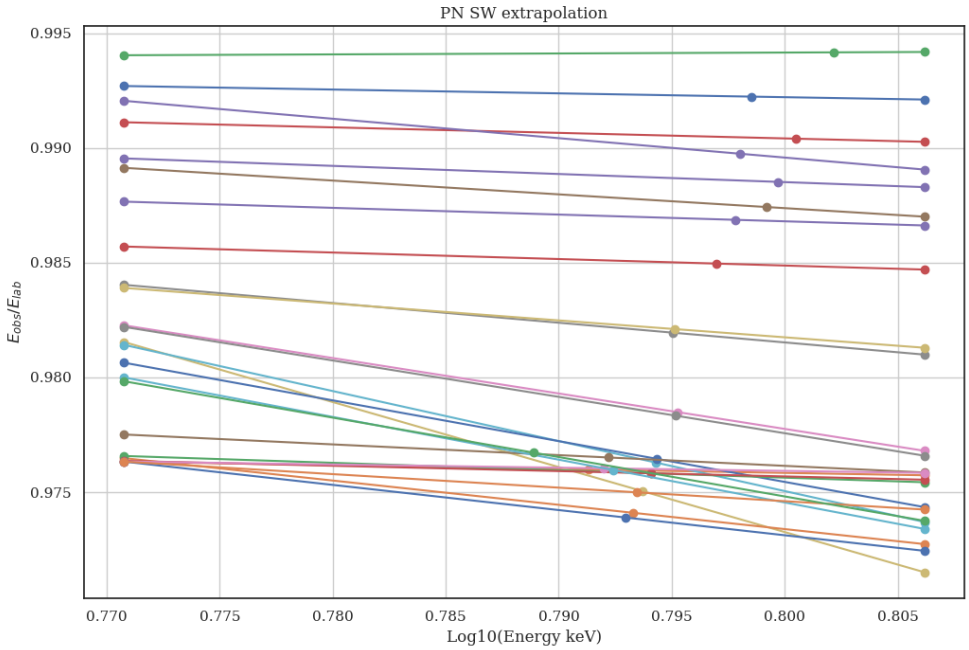

Figure 2: Extrapolation of the best-fit line centres E_{obs} for AGNs to E_{ref} = 6.4 keV (=0.8061 in $\log_{10}$) using the CC derived curve at 5.8988 keV (=0.7708 in $\log_{10}$). The spread of the points at 5.8988 keV is due to the different epochs of the AGN observations. All data points are from processing with the LTCTI turned off.

is performed linearly in log10(energy) space. Events with energies above 5.8988 keV are corrected with the value at 5.8988 keV. Events with energies below 1.486 eV are linearly interpolated down to zero for energy of 10 eV or less.

The XMM-SAS implementation requires that the long-term CTI should be encoded with the function $g(t)$ in

$$\mathrm{LTCTI}(t, E_{ref}, \mathrm{RAWY}) = E_{obs}/E'_{lab} = \left[\frac{1-g(t)}{1-a_0}\right]^{\mathrm{RAWY}}, \tag{2}$$

where t is the relative time in years since t_0, RAWY is the raw coordinate of the detector y-axis (the readout direction), a_0 is the CTI at $t = 0$ and its value is measured at launch using the calibration source, and $g(t)$ is a suitable function (see [4]); E_{ref} is the reference energy for the curve.

The XMM-SAS expects $g(t)$ for a set of reference energies and on a preselected set of times to be available in the `LONG_TERM_CTI` extension of the `EPN_CTI` calibration file. Consequently, we want to derive the best-fit $g(t)$ using the observed $\mathrm{LTCTI}(t, E_{ref}, \mathrm{RAWY})$. So, rewriting Eq. 2 we obtain:

$$g(t) = 1 - (1 - a_0) \times \mathrm{LTCTI}(t, E_{ref}, \mathrm{RAWY})^{1/RAWY}, \tag{3}$$

here a_0 and RAWY are fixed for each source included in the analysis.

For the AGNs in Small Window mode the average RAWY of the centre of the extraction region (always a circle with radius 32 arcsec) is 190 ± 1, so we assume RAWY=190 for all sources.

It is more complicated for the CC mode as we extract a box from the exposed CCD area, avoiding the edges. This includes events with RAWY from 137 to 200. The average RAWY for events within the Mn K_α line is 170.8 ± 0.4 for all CC observations and we use RAWY=170 in Eq. 2.

In previous version (v46 and earlier, see [4, 5, 6, 7]) the observed, non-CTI corrected line energies of Mn Kα were fit with a polynomial and this was used to derive $g(t)$ (via Eq. 2). However, this was not sufficient to describe the behaviour of the long-term effects, especially when adding the quiescent background correction (see [8]). Hence, in v47 and v48, $g(t)$ was tabulated and the actual

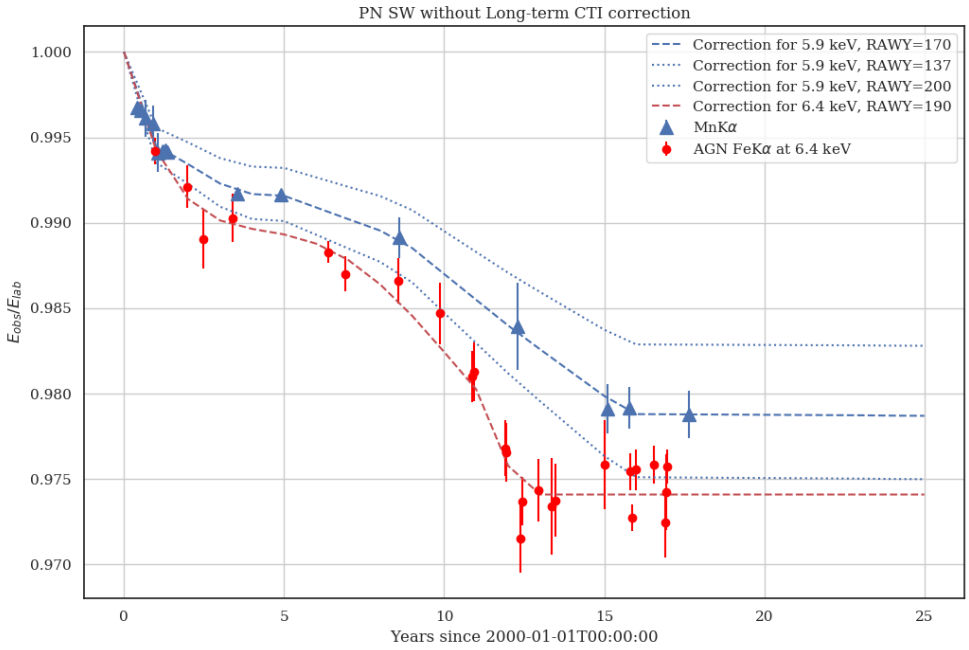

Figure 3: The ratio of E_{obs}/E'_{lab} for Mn Kα for *CalClosed* observation with PN in Small Window mode (blue triangles) and for a sample of AGNs with narrow Fe Kα line (red circles). The smooth curves used to derive $g(t)$ via Eq. 2-3 are shown in dashed blue for Mn Kα and in red for Fe Kα. The AGN ratios were extrapolated to 6.4 keV (see text for details). The two dotted lines represent the correction curve at 5.8988 keV at the two extreme RAWY for Small Window mode: 137 (upper curve) and 200.

model was a mixture of piece-wise linear or polynomial function and a suitable extrapolation for $t > 17$.

In this analysis we proceed in a slightly different way. We model the observed non-CTI corrected ratio $E_{obs}/E'_{lab} = \mathrm{LTCTI}(t, E_{ref}, \mathrm{RAWY})$ with a suitable smooth function and then derive $g(t)$ as in Eq. 3.

The reference energy E_{ref} is fixed to 5.8988 keV for the calibration source, while for the AGNs $E_{ref} = E_{obs}$ is different for each source because of the redshift (as listed in Table 1). To resolve this we incorporate an extrapolation to get LTCTI at a reference energy of 6.4 keV. This is done with a linear function in $\log(E)$ with two points: one at 5.8988 keV and one at E_{obs}. The point at 5.8988 is derived using linear interpolation on time for the epoch of the AGN observation. As XMM-SAS uses linear interpolation in $\log(E)$ space to derive the LTCTI for each event's energy, then this approach is correct. The extrapolation for all the AGNs in the sample is shown in Figure 2.

The observed non-CTI corrected $E_{obs}/E'_{lab} = \mathrm{LTCTI}(t, E_{ref}, \mathrm{RAWY})$ results are shown in Figure 3. The AGN points are extrapolated to 6.4 keV. Both model curves are based on a Univariate Spline function (from SCIPY.INTERPOLATE.UNIVARIATESPLINE in PYTHON, [2]). Once we have the LTCTI then we can derive the look-up table $g(t)$ using Eq. 3; $g(t)$ is calculated on a regular grid of years since t_0 with step 1 year and extrapolated out to $t = 25$. The extrapolation is just the value of $g(t)$ taken from the last datapoint.

Note that the extrapolation to 6.4 keV for the AGNs leads to a larger spread of the points on the E_{obs}/E'_{lab} axis. This large spread of points, especially at t>10 years as visible in Fig. 3, leads to large uncertainty for the smooth curve in this region. With some trial and error we tweaked the curve at a level of 0.1% in order to minimise the offset after applying the correction. Because of the interplay of the two energy points at 5.8988 and 6.4 keV it is not straightforward to obtain the best result by only considering changes in one of the curves.

Once we have $g(t)$ we can implement it in an updated CCF file. The changes to the long-term table in `EPN_CTI_0049.CCF` and `EPN_CTI_0050.CCF` with respect to the current versions are the

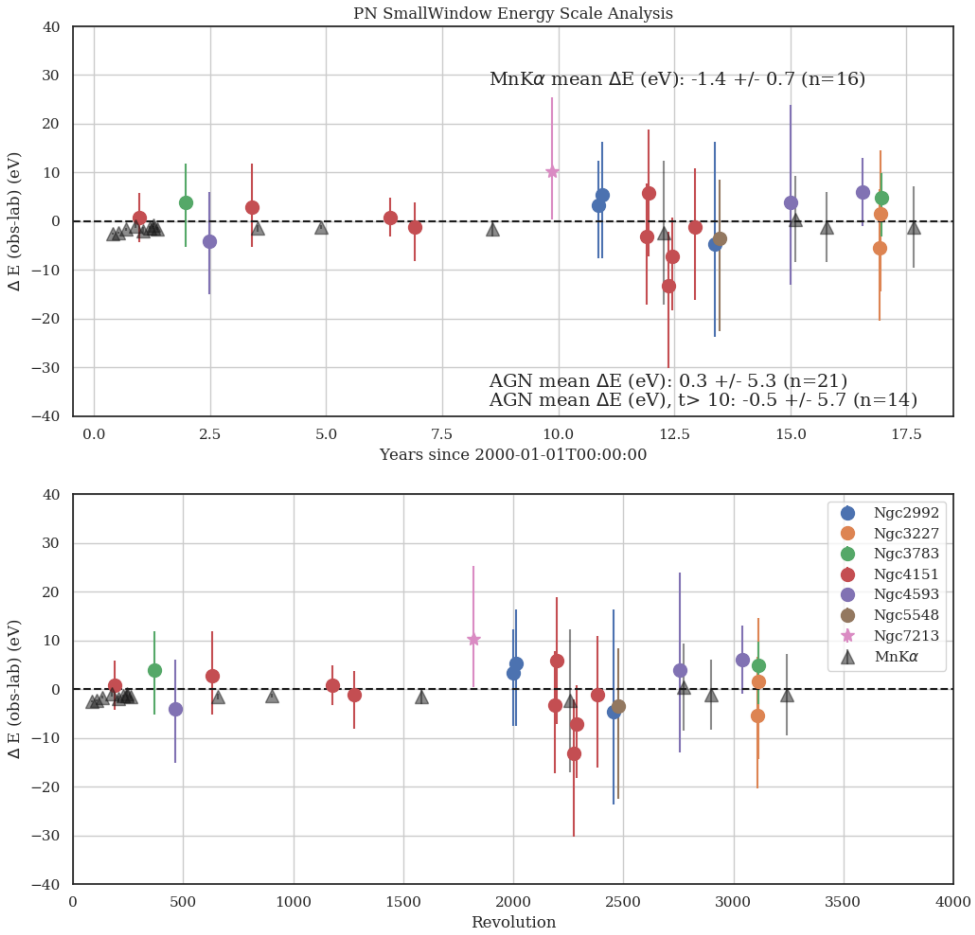

Figure 4: The results on the Mn Kα and Fe Kα lines after full reprocessing with `EPN_CTI_0049.CCF`. The y-axis is the difference of the best-fit line centroid and the expected line energy in eV. The mean difference and st.dev. for AGNs are annotated: including all epochs and for the most recent observations ($t > 10$ years).

following:

- Updated `T_COEFF` for `MODE_ID` = 3 at a reference energy of 5.8988 keV.
- Added a new line with `T_COEFF` for `MODE_ID` = 3 at a reference energy of 6.4 keV.

Note that if we do not implement a new reference energy point at 6.4 keV and only use the 5.8988 keV one, then the results for the AGNs are systematically off by $\Delta E \sim$ -30 eV for t $>$ 10.

4 Test Procedure

The results after applying the new correction, by repeating the analysis as outlined in Section 3.2, using the newly generated `EPN_CTI_0049.CCF`/`EPN_CTI_0050.CCF`, are shown in Figure 4. We see a significant improvement of the derived line energies for both the calibration source and the AGN sample.

5 Scientific Impact and Estimated Quality

For observations in PN-SW the new long-term CTI correction should provide improved energy scale for spectral features at 5.9–6.4 keV.

The quality, as measured from the mean and st.dev. of the results, is $\overline{\Delta E} = -1.4 \pm 0.7$ at 5.8988 keV and $\overline{\Delta E} = 0.3 \pm 5.3$ at 6.4 keV, as annotated in Figure 4.

6 Expected Updates

New PN-SW observations in CalClosed mode will be incorporated in updates to the Long-term CTI correction, if we see significant deviations. Similarly, new observations of AGNs with narrow Fe Kα line will be used to test the correction and the extrapolation. An update will be considered if the deviations are significant.

7 Caveats

- **Long-term CTI or gain effect?**
  The updated long-term CTI correction for the EPIC-pn Small Window mode is empirical. It is assumed that the observed systematic increase of the energy of the fitted line centres with time is due to a long-term CTI effect on the detectors and hence the deviation is modelled in such a way. The systematic shift to higher energies, however, could also be due in part to a gain effect caused by the quiescent background variations with time. For PN-SW we do not have enough area exposed to the background, which hampers the use of the discarded lines metadata as a proxy for the quiescent background (see [8]). Consequently we cannot distinguish between permanent changes of the CTI due to radiation damage and short or long-term temporal changes due to background variations.

- **Contaminating out-of-time events.**
  In both EPIC-pn window modes, the parts of the CCDs that are not read out are still exposed to the incoming X-rays, either from the sky or from the internal calibration source. When the selected window of the CCD is prepared for read out, it passes through the unexposed CCD area and into the frame-store for reading. The frame-store area is shielded from external X-ray photons. During this short transit, X-ray photons falling on the unexposed part of the chip will be superimposed on the actual observation – these are the so called out-of-time (OOT) events. The OOT fraction is usually much less than 10%. This effect is also present in observations of the calibration source and it is illustrated in great details in [1].
  For PN-SW in CalClosed mode, the OOT events will appear as if coming from RAWY between 137 and 200, while in reality they originate at RAWY < 137 (the unexposed part of the CCD). This effect is more pronounced in earlier epochs when the Iron-55 source is strong, as clearly seen in Fig. 5, (left-hand panel). The residual line between Mn Kα and Kβ, with an amplitude $\lesssim 10\%$ of the main line peak, is a manifestation of this effect. We consider the contamination not severe enough to bias any measurements of the line centroid of the Mn Kα line. In more recent epochs, as the Iron-55 source decays exponentially, the contribution is much smaller.
  The OOT events are also present in PN-SW observations of AGNs, but they will contribute mostly to the background as it is highly unlikely a very strong source at the same redshift as the target would fall in the "dark" area and bias the line centroid.

References

[1] Freyberg, M., 2006, EPIC-pn large window mode fast-shift CTI correction, XMM-Newton Calibration meeting, MPE

[2] Jones, E., Oliphant, E., Peterson, P., et al. SciPy: Open Source Scientific Tools for Python, 2001-, http://www.scipy.org/.

[3] Sanders, J. & Dennerl, K., 2017, Calibrating the EPIC-pn energy scale with the Cu fluorescent line, XMM-Newton Calibration meeting, Garching

[4] Smith, M.J.S, Guainazzi, M., Cappi, M., 2010, XMM-CCF-REL-271, EPIC-pn Long-Term CTI

[5] Smith, M.J.S, Guainazzi, M., Marinucci, A., 2013, XMM-CCF-REL-300, EPIC-pn Long-Term CTI

[6] Smith, M.J.S, Stuhlinger, M., Saxton, R.D., Freyberg, M.J., 2014, XMM-CCF-REL-323, EPIC-pn Long-Term CTI and Energy Scale

[7] Smith, M.J.S, 2016, XMM-CCF-REL-336, EPIC-pn Long-Term CTI

[8] Smith, M.J.S, Dennerl, K. & Freyberg, M.J., 2018, XMM-CCF-REL-358, EPIC-pn Energy Scale: Long-Term CTI and Quiescent Background Gain Correction.

Appendix

A Spectral fits of the CalClosed calibration source lines

Two examples of spectral fits for CalClosed observations: one from an earlier epoch and the most recent one.

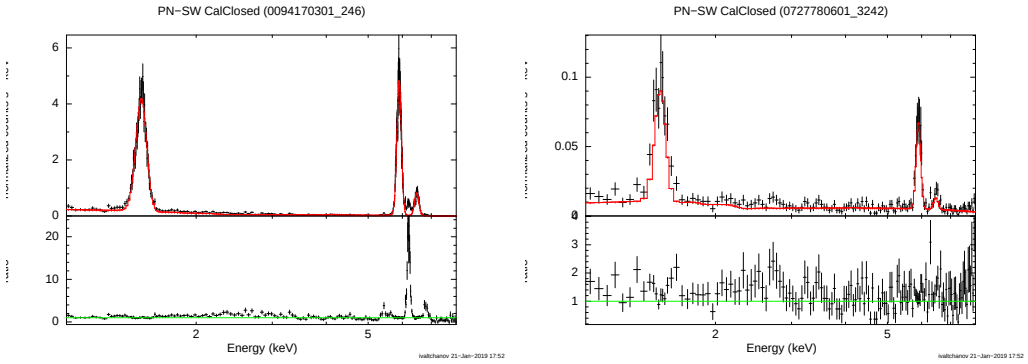

Figure 5: PN-SW in CalClosed: two examples for the XSPEC fit to the calibration source lines. Left: XMM-Newton revolution 246 ($t = 1.28$, top) and 3242 ($t = 17.653$, bottom). The upper panel of each plot shows the input data in black (binned only for visualisation purpose) in units of normalised counts/s/keV, in red is the best fit model, while the bottom panel is the ratio of data/model.

B Spectral fits of the AGNs Fe Kα line

Table 1: List of AGN targets included in the Fe K_α analysis. The redshifts are taken from Simbad. The expected observed energy of the Fe K_α line $E_{obs} = 6.399/(1+z)$ is indicated. The 21 observations included in the analysis are marked in boldface.

Name	Redshift	E_{obs}	Rev_OBSID
		keV	
ngc2992	0.007296	6.353	1906_654910301, 1911_654910401, 1916_654910501, 1921_654910601, **1999_654910701**, 2004_654910801, 2009_654910901, **2014_654911001**, **2458_701780101**
ngc3227	0.00386	6.374	3107_782520301, **3109_782520401**, 3110_782520501, 3112_782520601, **3114_782520701**
ngc3783	0.009755	6.337	193_112210101, **371_112210201**, 372_112210501, **3115_780860901**, 3120_780861001
ngc4151	0.003262	6.378	**190_112310101**, 633_143500101, **634_143500201**, 634_143500301, **1178_402660101**, **1277_402660201**, 2091_657840101, **2190_657840301**, **2197_657840401**, **2276_679780101**, **2290_679780201**, 2369_679780301, **2382_679780401**, 2917_761670101, 2918_761670201, 2919_761670301, 2921_761670501, 2922_761670601, 2934_761670701, 2935_761670801, 2937_761670901
ngc4593	0.008344	6.346	103_109970101, **465_59830101**, 2757_740920201, 2758_740920301, **2759_740920401**, 2760_740920501, 2761_740920601, **3040_784740101**
ngc5548	0.01627	6.297	191_109960101, 290_89960301, 291_89960401, **2479_720110301**, 2483_720110401, 2487_720110501, 2489_720110601, 2491_720110701, 2493_720110801, 2494_720110901, 2495_720111001, 2497_720111201, 2498_720111301, 2499_720111401, 2570_720111501, 2593_720111601, 2948_771000101, 2949_771000201
ngc7213	0.005867	6.362	**1818_605800301**

Table 2: XSPEC results for Fe K_α line fit. All fitting is done in energy range [4,8] keV and a model = "powerlaw + gausssian". The Gaussian line sigma is fixed and set to 10^{-3} keV (unresolved). $\Delta E = E - 6.4/(1+z)$, where z is the redshift of the galaxy. $\Delta E^{+,-}$ are the upper and lower 90% confidence level errors on the best fit line E. t_{exp} is the exposure time (in ksec) after filtering for high background periods. Δt is the time (in years) since 2000-01-01T00:00:00.

OBSID	Rev.	Δt [yr]	t_{exp} [ksec]	Line E [keV]	ΔE^- [keV]	ΔE^+ [keV]	ΔE [eV]	ΔE_{err} [eV]	C-stat	χ^2_r	D.O.F.
NGC 2992											
654910701	1999	10.8604	38.83	6.356	0.009	0.011	3.3	10.0	591.1	1.2923	595
654911001	2014	10.9425	42.02	6.358	0.011	0.013	5.3	12.0	640.2	1.3653	595
701780101	2458	13.3681	9.04	6.348	0.021	0.019	-4.7	20.0	614.0	1.499	595
NGC 3227											
782520401	3109	16.9248	56.81	6.369	0.012	0.015	-5.4	13.5	603.2	1.0406	595
782520701	3114	16.9520	53.97	6.376	0.013	0.016	1.6	14.5	616.7	1.0649	595
NGC 3783											
112210201	371	1.9658	50.5	6.341	0.008	0.009	3.8	8.5	647.6	1.0993	595
780860901	3115	16.9574	66.14	6.342	0.005	0.008	4.8	6.5	772.5	1.3535	595
NGC 4151											
112310101	190	0.9746	21.01	6.379	0.005	0.005	0.8	5.0	702.6	1.2501	595
143500201	634	3.4024	12.66	6.381	0.009	0.008	2.8	8.5	664.5	1.1485	595
402660101	1178	6.3761	27.98	6.379	0.004	0.004	0.8	4.0	856.0	1.5542	595
402660201	1277	6.9171	23.13	6.377	0.005	0.007	-1.2	6.0	737.4	1.284	595
657840301	2190	11.9073	5.82	6.375	0.011	0.014	-3.2	12.5	594.1	1.0511	595
657840401	2197	11.9456	6.59	6.384	0.013	0.013	5.8	13.0	622.6	1.0827	595
679780101	2276	12.3731	6.29	6.365	0.011	0.017	-13.2	14.0	720.8	1.2501	595
679780201	2290	12.4496	8.75	6.371	0.008	0.011	-7.2	9.5	667.1	1.207	595
679780401	2382	12.9526	6.64	6.377	0.012	0.015	-1.2	13.5	698.0	1.2352	595
NGC 4593											
59830101	465	2.4782	53.25	6.342	0.01	0.011	-4.0	10.5	666.5	1.1514	595
740920401	2759	15.0143	17.16	6.35	0.02	0.017	4.0	18.5	663.2	1.4317	595
784740101	3040	16.5474	98.48	6.352	0.007	0.007	6.0	7.0	681.0	1.1625	595
NGC 5548											
720110301	2479	13.4827	35.37	6.293	0.012	0.019	-3.6	15.5	638.1	1.2295	595
NGC 7213											
605800301	1818	9.8709	87.71	6.372	0.015	0.01	10.3	12.5	776.8	1.4019	595

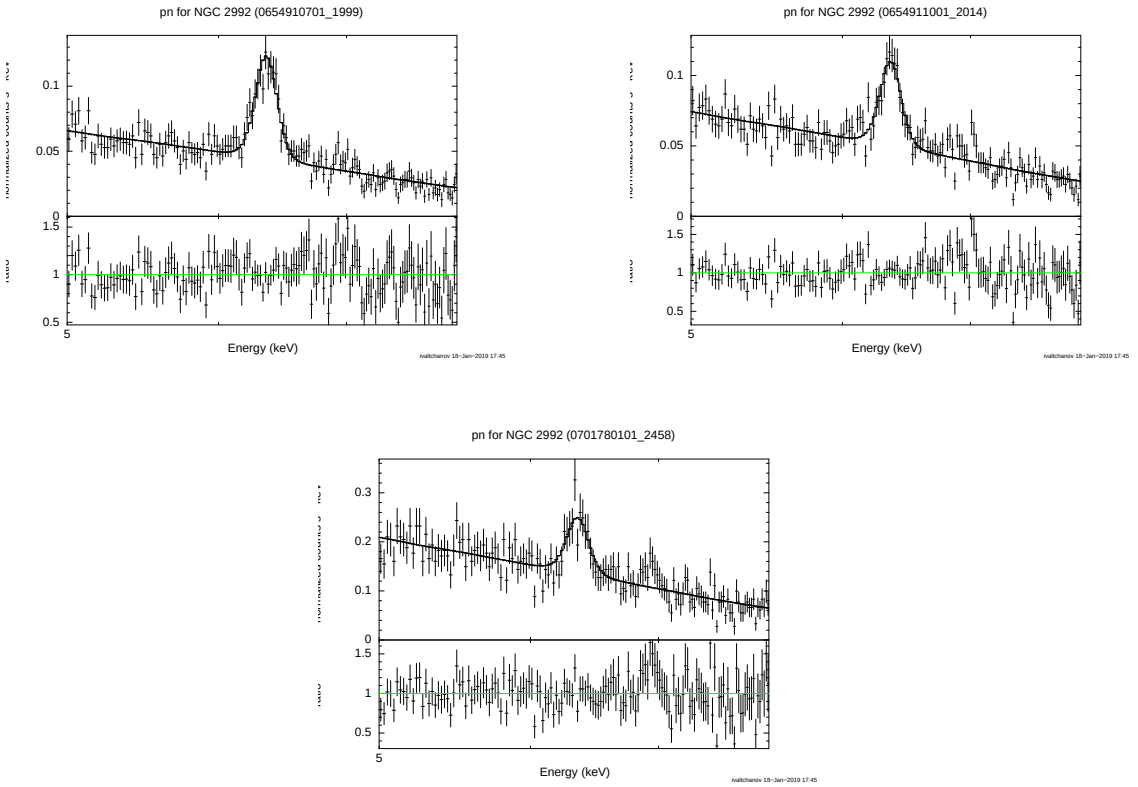

Figure 6: NGC 2992: Fe Kα fit results. The upper panel of each plot shows the input data with black symbols with error bars (the binning is only for visualisation purpose) in units of normalised counts/s/keV, the continuous black line is the best fit model, the bottom panel is the ratio of data/model.

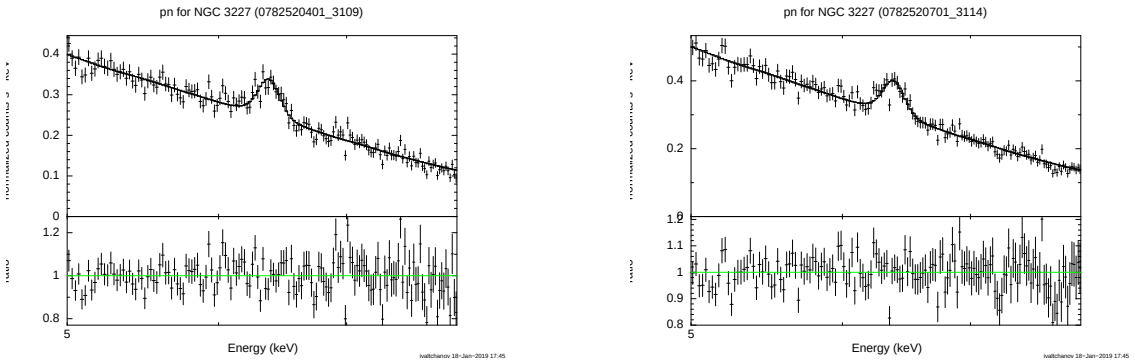

Figure 7: NGC 3227: Fe Kα fit results. See Fig. 6 caption for details.

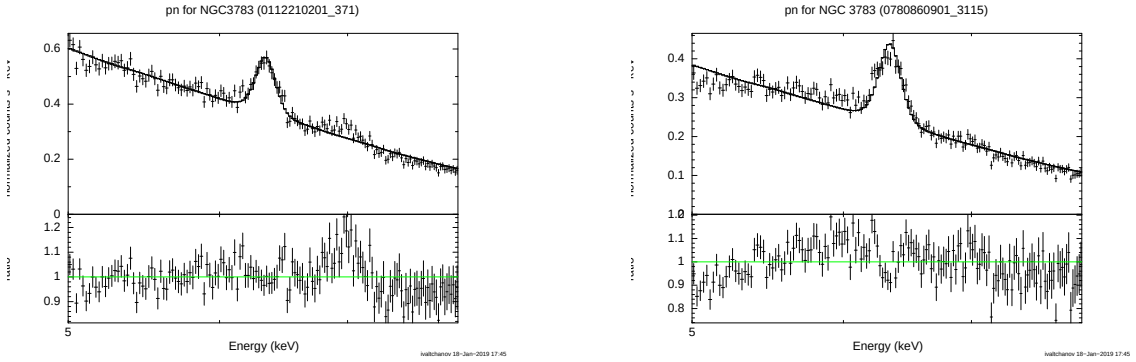

Figure 8: NGC 3783: Fe Kα fit results. See Fig. 6 caption for details.

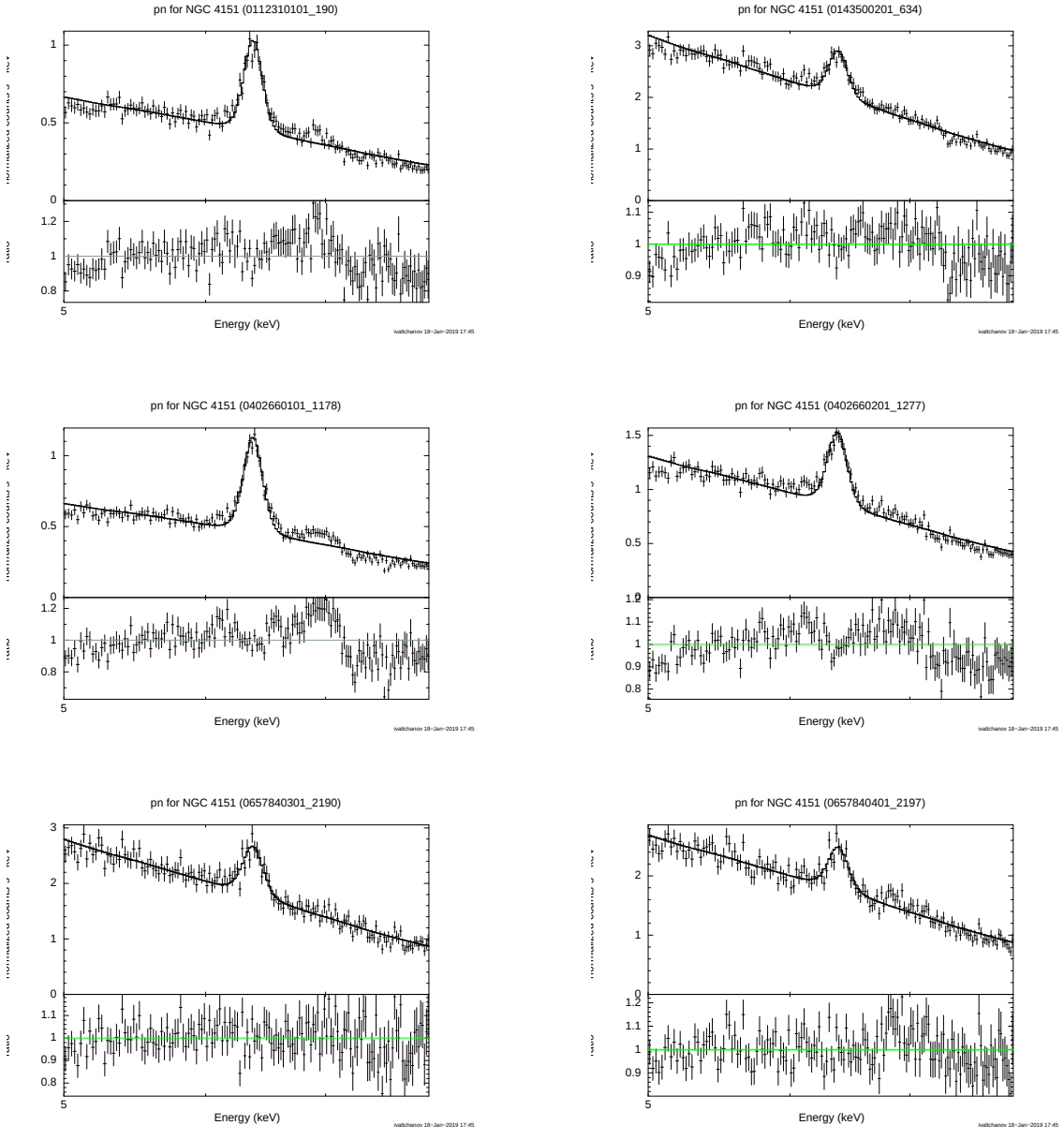

Figure 9: NGC 4151: Fe Kα fit results. Page 1. See Fig. 6 caption for details.

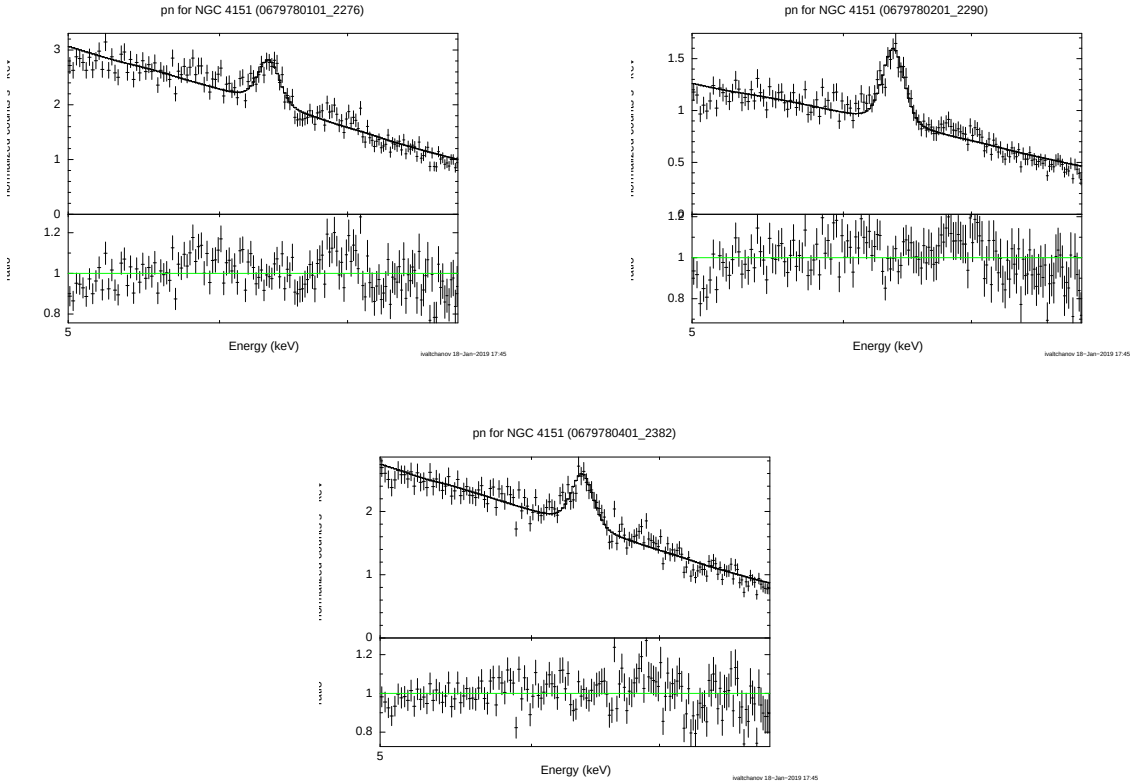

Figure 10: NGC 4151: Fe Kα fit results. Page 2. See Fig. 6 caption for details.

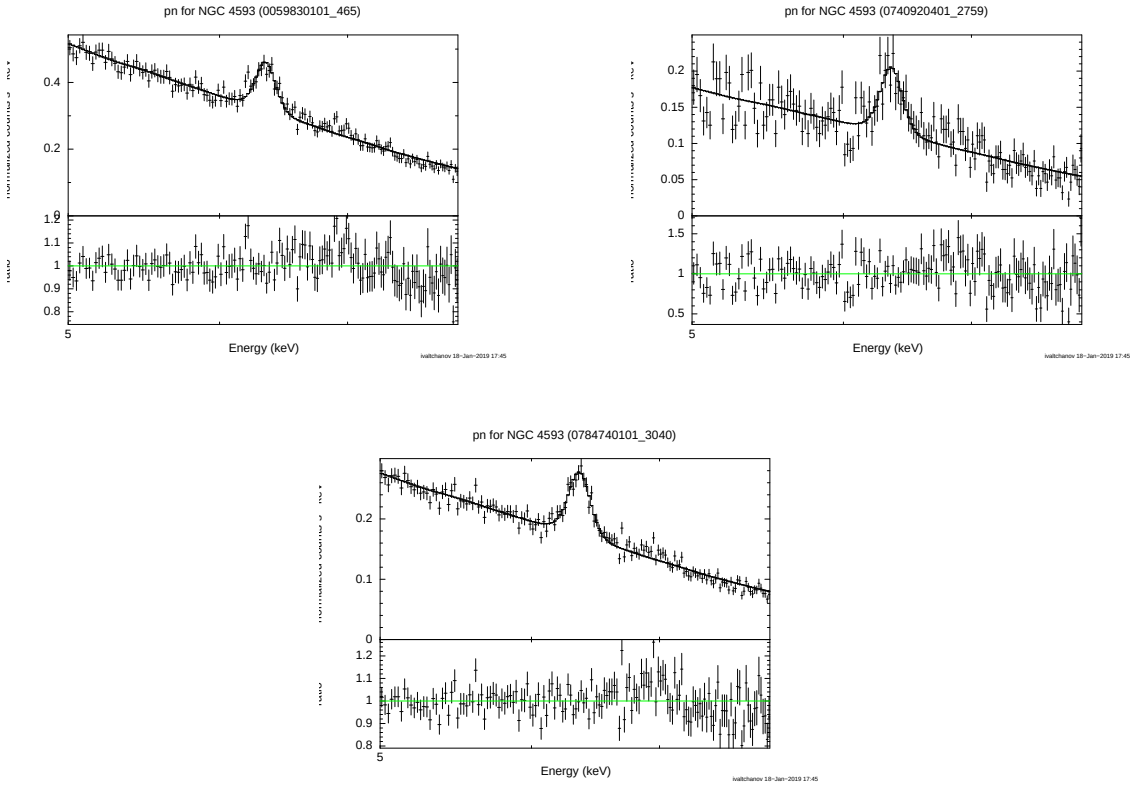

Figure 11: NGC 4593: Fe Kα fit results. See Fig. 6 caption for details.

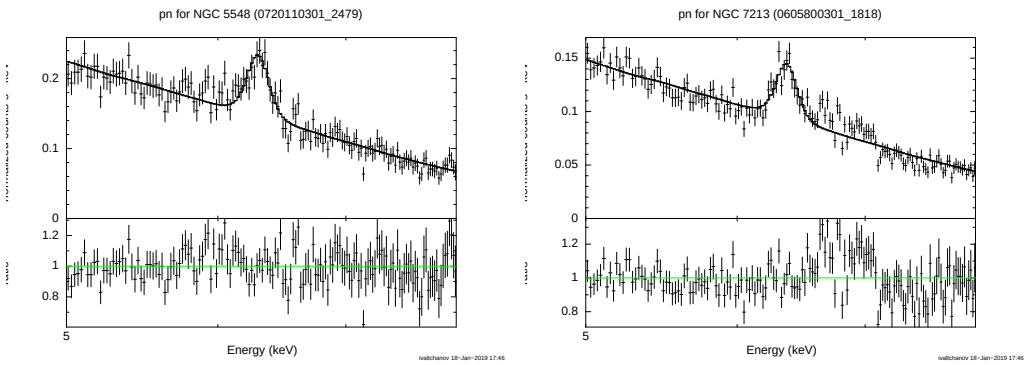

Figure 12: Fe Kα fit results for NGC 5548 (left) and NGC 7213 (right). See Fig. 6 caption for details.